Journal of Medical Engineering & Technology

ISSN: (Print) (Online) Journal homepage: https://www.tandfonline.com/loi/ijmt20

Analysis on diagnosing diabetic retinopathy by segmenting blood vessels, optic disc and retinal abnormalities

Ambaji S. Jadhav , Pushpa B. Patil & Sunil Biradar

To cite this article: Ambaji S. Jadhav , Pushpa B. Patil & Sunil Biradar (2020): Analysis on diagnosing diabetic retinopathy by segmenting blood vessels, optic disc and retinal abnormalities, Journal of Medical Engineering & Technology, DOI: 10.1080/03091902.2020.1791986

To link to this article: https://doi.org/10.1080/03091902.2020.1791986

Published online: 30 Jul 2020.

JOURNAL OF MEDICAL ENGINEERING & TECHNOLOGY
https://doi.org/10.1080/03091902.2020.1791986

Taylor & Francis
Taylor & Francis Group

REVIEW

Analysis on diagnosing diabetic retinopathy by segmenting blood vessels, optic disc and retinal abnormalities

Ambaji S. Jadhav[a], Pushpa B. Patil[b] and Sunil Biradar[c]

[a]Department of Electrical and Electronics, B.L.D.E.A's V.P. Dr. P.G. Halakatti College of Engineering & Technology (Affiliated to Visvesvaraya Technological University, Belagavi), Vijayapur, India; [b]Department of Computer Science & Engineering, B.L.D.E.A's V.P. Dr. P.G. Halakatti College of Engineering & Technology (Affiliated to Visvesvaraya Technological University, Belagavi), Vijayapur, India; [c]Department of Ophthalmology, Shri B.M. Patil Medical College Hospital and Research Center, Vijayapur, India

ABSTRACT

The main intention of mass screening programmes for Diabetic Retinopathy (DR) is to detect and diagnose the disorder earlier than it leads to vision loss. Automated analysis of retinal images has the likelihood to improve the efficacy of screening programmes when compared over the manual image analysis. This article plans to develop a framework for the detection of DR from the retinal fundus images using three evaluations based on optic disc, blood vessels and retinal abnormalities. Initially, the pre-processing steps like green channel conversion and Contrast Limited Adaptive Histogram Equalisation is done. Further, the segmentation procedure starts with optic disc segmentation by open-close watershed transform, blood vessel segmentation by grey level thresholding and abnormality segmentation (hard exudates, haemorrhages, Microaneurysm and soft exudates) by top hat transform and Gabor filtering mechanisms. From the three segmented images, the feature like local binary pattern, texture energy measurement, Shanon's and Kapur's entropy are extracted, which is subjected to optimal feature selection process using the new hybrid optimisation algorithm termed as Trial-based Bypass Improved Dragonfly Algorithm (TB – DA). These features are given to hybrid machine learning algorithm with the combination of NN and DBN. As a modification, the same hybrid TB – DA is used to enhance the training of hybrid classifier, which outputs the categorisation as normal, mild, moderate or severe images based on three components.

ARTICLE HISTORY
Received 27 January 2020
Accepted 28 May 2020

KEYWORDS
Diabetic retinopathy detection; optic disc; blood vessels; retinal abnormalities; trial-Based Bypass Improved Dragonfly Algorithm

1. Introduction

In present days, diabetes and its impediments are playing a crucial role in public health scenarios all over the world and the occurrence of diabetes is huge, which reaches very close as the epidemic [1,2]. Diabetic retinopathy (DR) is also named as diabetic eye disease, which is a significant symptom of diabetic microangiopathy and it is the common difficulties seen in diabetes patients. According to the growth of the disease, DR with 'early hidden, chronic progressive and irreversible features' are split into two kinds of 6, of which 1 to 3 to the normal retinopathy, 4 to 6 for the proliferative DR (PDR). Thus, early detection and prevention of DR are essential. Moreover, patients detected with 'Type-I and Type-II diabetes' have probability in suffering from DR [3]. In the first 5 years of diagnosis, the patients who are suffering from Type-I diabetes have approximately no chances of affecting from DR where the patients who are suffering from Type-II diabetes will have chances of suffering from DR [4–7].

The loss of vision may differ during the growth of DR. In general, DR is divided into two significant phases such as PDR, and non-proliferative DR (NPDR) that is classified by neovascularisation or vitreous/pre-retinal haemorrhage. Moreover, about 10% of diabetic patients who are not affected with DR will improve NPDR once a year, and for the patients with severe NPDR have the problem of improving PDR in that one year is 75%. In order to shift from regular status to PDR, it generally takes several years [8,9]. Therefore, NPDR is frequently split into three sub-categories like mild, moderate and severe. These five phases broadly utilise 'International Clinical Diabetic Retinopathy Disease Severity Scale' [10]. The treatment options are varied for the patients suffering in different stages of DR. Moreover, a retinal colour fundus image consisting of different structures like optic disc, red lesions, vascular tree and fovea, red lesions such as microaneurysms and haemorrhages [11]. Moreover, these microaneurysms and haemorrhages are assumed as

CONTACT Ambaji S. Jadhav asjadhavec@gmail.com Department of Electrical and Electronics, B.L.D.E.A's V.P. Dr. P.G. Halakatti College of Engineering & Technology, (Affiliated to Visvesvaraya Technological University, Belagavi), Vijayapur, India

dark lesions, while cotton wools and exudates are assumed as bright lesions [12].

In recent years, deep neural networks (DNNs) have attained revolutionary outcomes in several applications [3,13,14]. Several implementations of DNNs have established the performance, which will exceed beyond the human beings for example large scale visual recognition [15], the game of Go [16] and face recognition [17]. Moreover, the employment of DNNs for diagnosing DR has also attracted more attention, and more improvements were done. However, there are many improvements that were done, clinical application of automatic DR diagnosis model stays behind unavailable and several improvements need to be performed.

The critic contributions of the proposed DR detection model are portrayed as follows.

- To detect and treat DR at an early stage through optimal feature selection and classification model.
- To develop a new hybrid algorithm termed as Trial-based Bypass Improved Dragonfly Algorithm (TB – DA) to perform the feature selection and classification.
- To perform the classification with the hybridisation of two algorithms like deep belief network (DBN) and neural network (NN), with improved training algorithm, TB – DA.
- To certify and validate the ultimate performance of the optimal feature selection and classification-based DR detection model by analysing relevant performance measures.

The entire article is designed in the following manner: Section Literature review provides the literature review. Proposed model for diagnosing DR through different analysis is given in Section Proposed model for diagnosing DR through different analysis. Moreover, Section Steps adopted for various analysis shows the steps adopted for various analysis. Optimised hybrid classifier for detecting DR is given in Section Optimised hybrid classifier for detecting DR. The entire results and discussions are given in Section Results and discussions. The conclusion of the article is prearranged in Section Conclusion.

2. Literature review

2.1. Related works

In 2019, Sun [18] has implemented convolution neural network (CNN) technique to one-dimensional unrelated datasets and resolved the issue of data convolution of one-dimension. Moreover, the CNN method was merged with batch normalisation (BN) layer for averting the gradient scattering, improving the accuracy and training speed of the suggested method. The introduced method combined an adaptive learning rate model and optimised the technique. The test outcomes have shown that the proposed model attained high accuracy. Hence, it has been concluded that the developed method was not only suitable for DR diagnosis but also useful for other diseases like cardiovascular, cerebrovascular and chronic kidney diseases.

In 2019, Leeza and Farooq [19] had introduced an improved automated model for detecting the severity of DR that was a dictionary-based model and does not consist of pre-processing and post-processing phases. This method incorporated explicit pathological representation of the image into a training model. In order to categorise the images into five classes such as moderate, mild, proliferative DR, normal and severe non-proliferative DR, radial basis kernel support vector machine (SVM) and NN were employed. The suggested model has shown enhanced outcomes when compared over existing models.

In 2018, Costa et al. [20] have offered a new technique on the basis of multiple instance learning (MIL) for overcoming the requirements by leveraging the hidden data existing on annotations made at image level. Moreover, joint optimisation of instance encoding and the image classification steps were developed. In such a manner, helpful mid-level depictions of pathological images were acquired. The experimental results have proven that the suggested technique was highly suitable for detecting DR.

In 2018, Dashtbozorg et al. [21] have introduced a novel and consistent model for diagnosing Microaneurysms existing in retinal images automatically. At first, multiple preliminary microaneurysm persons were extracted by an iterative thresholding and a gradient weighting approaches. Next, a new set of features based on 'local convergence index filters' was extracted per each candidate along with the intensity and shape descriptors. By using six freely accessible datasets consisting of retinopathy online challenges (ROC) dataset, the proposed model was analysed. The results have proven that the suggested method was effective and robust in detecting microaneurysms with various resolutions and modalities.

In 2018, Wan et al. [20] have developed CNN for detecting DR that consisted of detection, segmentation and classification. Moreover, the suggested model

was merged with hyper-parameter tuning and transfer learning. In order to verify the image classification performance, VggNet, ResNet, AlexNet and GoogleNet were employed. The proposed model was analysed on freely accessible Kaggle platform for training. The outcomes have shown that the proposed model attained high accuracy.

In 2019 Gao et al. [22] have automated the DR detection and given suitable suggestions for DR patients, and constructed DR fundus images dataset, which were labelled using appropriate treatment approach. By this dataset, Deep CNN methods were trained for grading the severities of DR fundus images. The outcomes have shown that the suggested technique achieved high accuracy and effective.

In 2019, Kumar et al. [23] have presented Class-Enhanced Attentive Response Discovery Radiomics (CLEAR-DR) for diagnosing DR. Moreover, the 'CLEAR-DR' also provided a visual representation of the decision-making procedure along with the grading of disease using discovered deep radiomic sequencer for producing clear insight and knowledge of decision making procedure of the model. The efficiency and the usage of the suggested CLEAR-DR model were defined in improving the interpretability of grading outcomes to implement grading of DR. Thus, the suggested tool was highly potential in addressing the uninterpretability problem of CAD models. In 2016, Shaik et al. [24] have aimed for observing the hybrid method was introduced by a hybrid morphological reconstruction method for pre-processing using watershed segmentation approach as post-processing was suggested.

2.2. Review

Though there are several methods for detecting DR, still new methods need to be implemented for overcoming the existing drawbacks. Table 1 describes some of the existing DR detection approaches. Among them, CNN [18,20] is used to solve the issue of one-dimensional irrelevant data convolution, it increases the accuracy and training speed, it does not need feature extraction, and it has attained high accuracy. But, there are few disadvantages such as the significant problem with this method is overfitting, it is highly expensive, and when GPU was not good, CNN's are very slow to train. Moreover, NN [19] has attained high sensitivity and specificity, and it consumes less time. But, it has some conflicts like it is computationally expensive, and it still uses black box testing. MIL [25] is automatically employed for instance classification tasks, and it has high performance. Yet, it there are no particular classes for instances, it will not work well. Random Undersampling Technique Boost (RUSBoost) [21] is used to enhance the performance on unbalanced data, and it is an appropriate classifier for skewed set with more non-microaneurysms and less microaneurysms candidates. However, it eliminates the helpful information. Deep CNN [22] has improved performance on image tasks, and it is employed to detect lesions from the fundus images. But, when GPU was not good, CNN's are very slow to train. CLEAR-DR [23] is a powerful tool for solving the uninterpretability risk, and it has high accuracy and reliability. Yet, it needs to improve the performance. Watershed segmentation [24] has high speed operation, and it is noise resistance. Still, it is highly

Table 1. Features and challenges of existing diabetic retinopathy detection models.

Author [citation]	Methodology	Features	Challenges
Sun [18]	CNN	• It is used to solve the issue of one-dimensional irrelevant data convolution. • It increases the accuracy and training speed.	• The significant problem with this method is over fitting. • It is highly expensive.
Leeza and Farooq [19]	NN	• Has attained high sensitivity and specificity. • Consumes less time.	• It is computationally expensive. • It still uses black box testing.
Costa et al. [25]	MIL	• It is automatically employed for instance classification tasks. • Has high performance.	• If there are no particular classes for instances, it will not work well.
Dashtbozorg et al. [21]	RUSBoost	• It is used to enhance the performance on unbalanced data. • It is an appropriate classifier for skewed set with more non-microaneurysms and less microaneurysms candidates.	• It eliminates the helpful information.
Wan et al. [20]	CNN	• It does not need feature extraction. • Has attained high accuracy.	• When GPU was not good, CNN's are very slow to train.
Gao et al. [22]	Deep CNN	• Has improved performance on image tasks. • It is employed to detect lesions from the fundus images.	• It requires huge amount of data.
Kumar et al. [23]	CLEAR-DR	• It is a powerful tool for solving the uninterpretability risk. • Has high accuracy and reliability.	• Need to improve the performance.
Shaik et al. [24]	Watershed segmentation	• Has high speed and it is noise resistance. • Has high performance.	• It is highly sensitive to local minima.

sensitive to local minima. Therefore, it has been demonstrated that the above-specified challenges are useful for developing a new model in an efficient manner.

3. Proposed model for diagnosing DR through different analysis

3.1. Proposed architecture

In the earlier years, many efforts have been made for reducing the difficulties of detecting DR. However, with those existing methodologies, there have been some defects for detecting the disease at an early stage. In that case, a new model is introduced in this article for diagnosing DR effectively through various analyses, where the architectural depiction is shown in Figure 1.

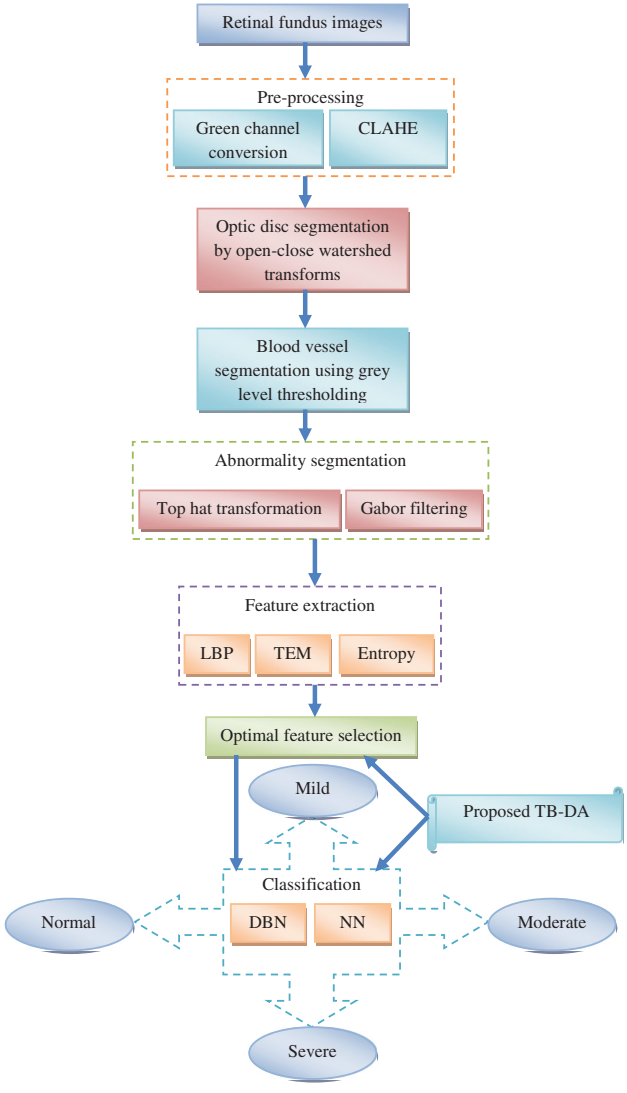

Figure 1. Proposed architecture of developed diabetic retinopathy detection using various stages.

The proposed DR detection model consists of several stages such as 'image pre-processing, optic disc segmentation, blood vessel segmentation, feature extraction, optimal feature selection and classification'. Initially, the pre-processing stage takes retinal fundus image as the input and performs green channel conversion and Contrast Limited Adaptive Histogram Equalisation (CLAHE) for enhancing the contrast of the image. Next, the optic disc segmentation is done by open-close watershed transform. The watershed method is a mathematics model, which is used for image segmentation on the basis of region processing with several benefits. Further, the optic disc segmented image is subjected to blood vessel segmentation, which is done by grey level thresholding. Next to the segmentation of optic disc and blood vessels, abnormality segmentation is done using top hat transform and Gabor filtering mechanisms. Moreover, this research work focuses on the analysis of DR detection by observing the optic disc, blood vessels and segmented abnormalities like 'hard exudates, haemorrhages, Microaneurysm and soft exudates'. Hence, each segmented image is subjected for feature extraction using local binary pattern (LBP), texture energy measurement (TEM) and entropy. In order to reduce the length of the features after feature extraction, optimal feature selection is developed by the proposed hybrid TB – DA. The extracted features are subjected to the machine learning algorithm with the combination of DBN and NN. Moreover, in the hybrid classifier, the weight update of both NN and DBN is optimised by the same TB – DA as a new training algorithm, which categorises the image into normal, mild, moderate or severe on the basis of three component analysis. The main intention of the developed TB – DA in optimal feature selection is to minimise the correlation between the selected features, and weight update in hybrid classifier is to minimise the error difference between measured and target output.

The input retinal image is represented as ZE^{input}, which is again denoted as $ZE^{\text{pre-process}}$ after pre-processing. Further, ZE^{optic}, and $ZE^{\text{optic}*}$ signify the optic disc segmented image and optic disc removed images, respectively, ZE^{vessel}, and $ZE^{\text{vessel}*}$ signify the blood vessel segmented image, and blood vessel removed image, respectively, and $ZE^{\text{abnormality}}$ signifies the abnormality segmented image. Further, the extracted features are represented as $ZFit_{le}$, where $le = 1, 2, \ldots, NZ$, and NZ is the number of extracted features involves LBP, TEM and entropy in all three components like optic disc, blood vessels and abnormalities.

3.2. Objective model

There are mainly two objectives that need to be solved by the proposed DR detection model. The first one is optimal feature selection and second one is classification. In the optimal feature selection, the objective model is to minimise the correlation between the selected features by developed TB – DA. Equation (1) derives the correlation among the two features AE and BE, where N_E indicates the number of feature pairs.

$$\mathrm{Cor} = \frac{N_E \sum AE.BE - \sum AE \sum BE}{\sqrt{\left(N_E \sum AE^2 - \left(\sum AE^2\right)\right) - \left(N_E \sum BE^2 - \left(\sum BE^2\right)\right)}} \quad (1)$$

Hence, the minimised correlation function under optimal feature selection is given in Equation (2).

$$\mathrm{FF1} = \underset{\{ZFit_1, ZFit_2, \ldots, ZFit_{NZ}\}}{\operatorname{argmin}} (\mathrm{Cor}) \quad (2)$$

Moreover, the second objective model for the proposed DR diagnostic model is to minimise the error difference between the measured and classified outcome of DBN and NN through optimal training (weight updating) by TB – DA. When the original output vector is indicated by C^r, and the measured outcome DBN and NN is denoted as D^r, the error function among the measured and target outcome is given in Equation (3). Hence, the objective function of optimal classification is based on Equation (4).

$$\mathrm{ER} = C^r - D^r \quad (3)$$

$$\mathrm{FF1} = \underset{\{W_n^{NN}, W_n^{DBN}\}}{\operatorname{argmin}} (ER) \quad (4)$$

Hence, the proposed TB-DA is used to attain the better performed DR detection with optimal feature selection and classification.

4. Steps adopted for various analysis

4.1. Image pre-processing

In the proposed DR detection model, the pre-processing procedure is done by green channel conversion, and CLAHE.

Green Channel: Here, RGB image is considered as the input retinal fundus image, which consists of three channels like red, green and blue, which are converted to green channel image. In general, the RGB images are low brightness images, whereas the green channel images are high brightness images, from which the abnormalities could be clearly observed.

CLAHE: This process is used to enhance the contrast of the image. The algorithmic representation of the CLAHE-based contrast enhancement of the image is based on [26]. Once contrast enhancement is done, the pre-processed image is denoted as $ZE^{\mathrm{pre-process}}$ and it is subjected to watershed transform for segmenting the optic disc.

4.2. Optic disc segmentation

Here, the segmentation of optic disc is performed by open-close watershed transformation [27]. In order to eliminate optic disc from the pre-processed image, watershed transformation follows few steps such as at first, the image is read to segment. Once the image is read, the structure element of the read image is defined. Later, morphological dilation followed by opening–closing is done. Moreover, the background markers are computed, which are given to watershed transformation. Furthermore, the function is subjected for performing quantitative evaluation. An open-close or close-open watershed approach is employed for dealing with the dark and the bright lesions. The mathematical formula for morphological opening of the image $ZE^{\mathrm{pre-process}}$ by a structural element SE is denoted in Equation (5), and the respectively closing function is represented in Equation (6).

$$ZE^{\mathrm{optic}} = ZE^{\mathrm{pre-process}} \circ SE = (ZE^{\mathrm{pre-process}} \Theta SE) \oplus SE \quad (5)$$

$$ZE^{\mathrm{optic}} = ZE^{\mathrm{pre-process}} \bullet SE = (ZE^{\mathrm{pre-process}} \oplus SE) \Theta SE \quad (6)$$

Moreover, the watershed line refers to a function that is the collection of points of a function which is not belonged to any other catchment basin and the corresponding equation is expressed in Equation (7).

$$W_{\mathrm{sh}}(f) = \mathrm{sp}(f) \cap \left[\bigcup_t \left(\mathrm{cb}(\mathrm{rgm}_t)\right)\right]^o \quad (7)$$

In the above equation, the support to the function f is denoted as $\mathrm{sp}(f)$ and the catchment basin with the regional minima (rgm_t) is denoted as $\mathrm{cb}(\mathrm{rgm}_t)$. Once the watershed ridge lines are computed, the intensity of the image is altered using morphological recreation thus it has the regional minima in required locations. The output image $ZE^{\mathrm{optic}*}$ is later subjected for segmentation of blood vessels in an efficient manner.

4.3. Blood vessel segmentation

In this section, the blood vessels are segmented from the image ZE^{optic}. This is done by grey level thresholding [28] that works based on the assumption of that image has bimodal histogram. Therefore, from the background, the object is considered by simple process that

compares the image with threshold *tl* value that divides into two modes and the output threshold image is given in Equation (8), and this is referred as the binary image.

$$\mathrm{ZE}^{\mathrm{vessel}} = \begin{cases} 1 & \text{if } \mathrm{ZE}^{\mathrm{optic}*}(i,j) > tl \\ 0 & \text{if } \mathrm{ZE}^{\mathrm{optic}*}(i,j) \leq tl \end{cases} \tag{8}$$

In the above equation, the pixel with intensity value 1 denotes the object and 0 denotes the background. Thus, the segmented blood vessel image is denoted as ZE^{vessel} and the blood vessel removed image $ZE^{\mathrm{vessel}*}$ is given for abnormality segmentation.

4.4. Abnormality segmentation

The abnormalities of retinal image like hard exudates, haemorrhages, Microaneurysm and soft exudates are segmented by top hat transform, and Gabor filtering.

a. *Top Hat Transform* [29]: This is defined as the variance among the actual and the image opening. The main intention of this model is to lighten the objects on the dark background, which results in improving the brightness of the image. In addition, top hat transform of the image $ZE^{\mathrm{vessel}*}$ is shown in Equation (9). Here, the structuring element is denoted as SE.

$$\mathrm{TH}(\mathrm{ZE}^{\mathrm{vessel}*}) = \mathrm{ZE}^{\mathrm{vessel}*} - (\mathrm{ZE}^{\mathrm{vessel}*} \circ \mathrm{SE}) \tag{9}$$

b. *Gabor Filtering* [30]: It is generated from two elements called Gaussian and sinusoidal, which has the ability of connecting the optimal depiction of spatial domain and the orientation direction. The numerical equation denoting the Gabor filtering of the image is expressed in Equation (10).

$$gf(y,z;\theta,fq) = \exp\left\{-\frac{1}{2}\left[\frac{y_{\theta'}^2}{\sigma_y^2} + \frac{z_\theta^2}{\sigma_z^2}\right]\right\}\cos(2\Pi fq y_\theta) \tag{10}$$

In the above equation, *fq* denotes the cosine wave frequency along *y* and *z* axes, the fixed distance from Gaussian properties is denoted as σ_y and σ_z, respectively. The orientation direction is denoted as θ. In addition, the representation of y_θ and z_θ is shown in Equations (11) and (12), respectively.

$$y_\theta = y\cos\theta - z\sin\theta \tag{11}$$

$$z_\theta = y\sin\theta + z\cos\theta \tag{12}$$

Finally, the term $\mathrm{ZE}^{\mathrm{abnormality}}$ denotes the abnormality segmented image and it is further given for the feature extraction in order to extract consistent features.

4.5. Feature extraction

The feature extraction is performed by three approaches such as LBP, (2) laws texture energy (LTE), and (3) Entropy.

(a) *LBP* [31]: This is suggested as effective and strong texture descriptor that will be applied to broad range of applications from texture segmentation to face recognition. The histogram of the labelled image $ZE^{\mathrm{abnormality}}(x,y)$ is employed as a descriptor and it is denoted in Equation (13), where $I(\mathrm{SE}) = 1$, if SE is true, and $I(\mathrm{SE}) = 0$ if SE is false, and the count of different labels produced by the LBP operator is denoted as *nl*.

$$Hg_{im} = \sum_{x,y} I(\mathrm{ZE}^{\mathrm{abnormality}}(x,y) = im), im = 0, \ldots, nl-1 \tag{13}$$

In addition, a circular neighbourhood is considered around a pixel. On the circumference of the circle, points *po* are chosen with radius *ra*. Equation (14) denotes the uniformity metric UN as *po*-bit binary number $(s_{po-1}, s_{po-2,} \cdots, s_1, s_0)$. The rotation invariant uniform pattern *UN* value is less than or equal to 2 is denoted in Equation (15).

$$\mathrm{UN}(\mathrm{LBP}_{po,ra}) = \left|s_{po-1} - s_0\right| + \sum_{po=1}^{po-1}\left|s_{po} - s_{po-1}\right| \tag{14}$$

$$\mathrm{LBP}_{po,ra} = \begin{cases} \sum_{co=0}^{po-1} Z(gv_{cpo} - gv_{cpx}) & \text{if } \mathrm{UN}(\mathrm{LBP}_{po,ra}) \leq 2 \\ po+1 & \text{Otherwise} \end{cases} \tag{15}$$

In Equation (15), the grey values of the centre pixel is indicated by gv_{cpx}, and the grey values of points *po* is expressed as $gv_{cpo}, co = 0, \ldots, po-1$.

(b) *LTE* [32]: This is one of the regularly used texture descriptors that are used in distinct implementations including medical image analysis. In addition, the overall masks are obtained from one dimensional vector with five pixel lengths *L5*, *S5*, *E5*, *R5* and *W5* denotes the level detection, spot detection, edge detection, ripple detection and wave detection, respectively. In order to extract the texture data from $\mathrm{ZE}^{\mathrm{abnormality}}(x,y)$, the image is elaborated with each two-dimensional mask. If the filter *L5E5* is taken into consideration, then obtained texture image is denoted in Equation (16).

$$\mathrm{TEX}_{L5E5} = \mathrm{ZE}^{\mathrm{abnormality}}(x,y) \otimes L5E5 \tag{16}$$

The texture image TEX_{L5L5} is used for normalising the brightness of the other texture images $TEX(x,y)$ and the corresponding equation is denoted in Equation (17). Moreover, the appropriate convolution of these masks generates 25 distinct combinations. The outcomes are given to TEM that consisting of moving non-linear window average of absolute values as given in Equation (18).

$$\text{Normalize}\left(\text{TEX}_{(x,y)}\right) = \frac{\text{TEX}_{(x,y)}}{\text{TEX}_{(x,y)^{L5L5}}} \tag{17}$$

$$TEM_{(x,y)} = \sum_{c=-7}^{7}\sum_{d=-7}^{7}\left|TEX_{(x+cy+d)}\right| \tag{18}$$

Moreover, a 14 rotationally in variant TEM (TR) is acquired by combining 25 TEM descriptors and the mathematical equation is shown in Equation (19).

$$\text{TR}_{E5L5} = \frac{\text{TEM}_{E5L5} + \text{TEM}_{L5E5}}{2} \tag{19}$$

(c) *Entropy* [33]: This can be determined as the uncertainty association with randomness. In this, two different types of entropy's are taken into assumption like Shannon and Kapur's entropy methods. Let, the input segmented image $\text{ZE}^{\text{abnormality}}(x,y)$ includes N_{dsg} distinct grey values. Therefore, the normalised histogram is defined to the specific region of interest of size $(ne \times me)$ is denoted in Equation (20).

$$\text{Entropy}_{dsg} = \frac{N_{dsg}}{ne \times me} \tag{20}$$

Moreover, the Shannon entropy's equation is denoted in Equation (21), whereas the equation related to Kapur's entropy is given in Equation (22) that has high dynamic range than the Shannon entropy over a range of scattering situations, and it is useful in evaluating scatter regularity and density. The whole features taken are at last denoted as FR_{in} and it is given in Equation (23).

$$\text{SHE} = -\sum_{dsg=0}^{M-1}\text{Entropy}_{dsg}\log_2\left(\text{Entropy}_{dsg}\right) \tag{21}$$

$$\text{KE}_{\alpha,\beta} = \frac{1}{\beta-\alpha}\log_2\frac{\sum_{dsg=0}^{M-1}\text{Entropy}_{dsg}^{\alpha}}{\sum_{dsg=0}^{L-1}\text{Entropy}_{dsg}^{\beta}} \tag{22}$$

$$\text{FR}_{\text{in}} = \text{LBP}_{po,ra} + \text{TEM}_{(x,y)} + \text{SHE} + \text{KE}_{\alpha,\beta} \tag{23}$$

Therefore, the combinations of all features are denoted as $ZFit_{le}$, which are further subjected for feature selection by proposed TB – DA in order to select the unique features with minimum correlation.

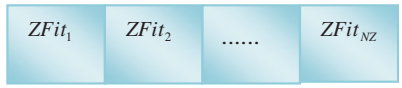

Figure 2. Solution encoding for optimal feature selection.

4.6. Optimal feature selection

Here, the optimal features are selected from the input features $ZFit_{le}$ using the improved TB – DA model that selects the optimal features $ZFit_{le*}$. The solution encoding for optimal feature selection is shown in Figure 2.

5. Optimised hybrid classifier for detecting DR

5.1. Conventional heuristics

5.1.1. DA

The conventional DA [34] algorithm is inspired by the swarms behaviour that is either static or dynamic. Moreover, the entities of the swarm should search for the food and reroute the enemies. On the basis of traditional DA, there are five key factors that need to be assumed for updating the individual's position. The significant factors such as 'cohesion, alignment, separation, attraction and distraction' are the behaviours of the dragonflies. The separation of ath dragonfly, Sp_a constructs its neighbours based on Equation (24).

$$Sp_a = -\sum_{b=1}^{Nd}(Y - Y_b) \tag{24}$$

In the above equation, the number of neighbouring individuals is denoted as Nd, the location of the current individual is represented as Y and the location of bth neighbouring individual is denoted as Y_b. The separation of ath individual is denoted as Sp_a. Moreover, the alignment is measured by Equation (25).

$$Ag_a = \frac{\sum_{b=1}^{Nd}Vl_b}{Nd} \tag{25}$$

In Equation (25), the velocity of bth individual is indicated by Vl_b. The alignment of ath individual is indicated by Ag_a. In addition, Equation (26) represents the control cohesion, in which the alignment of ath individual is denoted as Ch_a. The attraction towards food is computed by Equation (27), and the distraction towards enemy is measured by Equation (28).

$$Ch_a = \frac{\sum_{b=1}^{Nd}Y_b}{Nd} - Y \tag{26}$$

$$At_a = \text{Food} - Y \tag{27}$$

$$Ds_a = \text{Enemy} + Y \tag{28}$$

In Equations (27) and (35), the position of the food source is denoted as Food, whereas the position of the enemy is denoted as Enemy. The source of food of ath individual is represented as At_a, and the position of enemy of ath individual is indicated by Ds_a.The movement of each dragonfly is determined using step vector, which could be done by Equation (29).

$$\Delta Y_{tm+1} = (spSp_a + agAg_a + chCh_a + atAt_a + dsDs_a) + \delta \bullet \Delta Y_{tm} \tag{29}$$

In Equation (29), the current iteration is denoted as tm, the weight of separation, alignment, cohesion, attraction and distraction are indicated by sp, ag, ch, at and ds, respectively. Moreover, the weight of inertia is given by δ. Equation (30) specifies the position vector. When there is no neighbouring solution, the dragon fly has to move around the search space using random walk on incrementing the randomness, stochastic characteristics and exploration.

$$Y_{tm+1} = Y_{tm} + \Delta Y_{tm+1} \tag{30}$$

The positions of the dragonflies have to update its solution by Equations (31) and (32). Here, the position vector is denoted as PV, the random numbers ranging from 0 to 1 is denoted as rd_1 and rd_2, and the term ξ denotes constant. By measuring the Euclidean distance among all the dragonflies, the neighbourhood of the individual dragonfly is determined and later, the position and the step vectors are updated.

$$Y_{tm+1} = Y_{tm} + \text{Levy}(\text{PV}) \times Y_{tm} \tag{31}$$

$$\text{Levy}(\text{PV}) = 0.01 \times \frac{rd_1 \times \varphi}{|rd_2|^{\frac{1}{PV}}} \tag{32}$$

$$\varphi = \left(\frac{\Gamma(1+\xi) \times \sin\left(\frac{\Pi\xi}{2}\right)}{\Gamma\left(\frac{1+\xi}{2}\right) \times \xi \times 2^{\left(\frac{\xi-1}{2}\right)}} \right)^{\frac{1}{\xi}} \tag{33}$$

$$\Gamma(r) = (r-1)! \tag{34}$$

5.1.2. ROA

The inspiration of Rider Optimisation Algorithm (ROA) [36] is based on the group of riders that are going in the direction of destination. Let, a few riders groups are going towards the same target for winning the race. In the conventional ROA, there are four rider's groups that are considered, in which the count of riders should be same in all the four groups. Bypass rider, followers, overtakers and attackers are the four groups of riders.

5.1.3. Parameter initialisation for rider and group

At first, four rider's clusters need to be initialised and it is denoted as G and their locations must be initialised randomly. In addition, steering, accelerator acr, gear gr and brake bk are the rider parameters that need to be initialised once the group initialisation is done.

5.1.4. Determining the leading rider

For finding the leading rider, success rate is taken into consideration.

5.1.5. Update the location of riders

In order to find the leading rider and winner of the race, the rider's location in each group is updated each time. The bypass riders will not follow the process of leading riders because they have their own path and the update process of this rider is shown in Equation (35).

$$Y^{br}_{tm+1} = \delta\left[Y_{tm}(\eta, h) * \beta(h) + Y_{tm}(\xi, h) * [1 - \beta(h)]\right] \tag{35}$$

In Equation (35), the random values in between [0, 1] is denoted as δ and β. Similarly, the random value ranging from 0 to rn is indicated by η and ξ. Moreover, the size of β is $1 \times cn$. Thus, every rider in the cluster will update the location and become as a winner. Further, the follower, overtaker and attack riders are updated based on [36].

5.1.6. Determining the success rate

Once the update process is done, each rider's success rate is computed. Thus, the rider with maximum success rate will be termed as the leading rider.

5.2. Proposed TB – DA

Even though DA [34] performs well in complex optimisation problems, it suffers from few defects like the overflowing of search space and the interruption of random flights since it has huge searching stages. In order to improve the LFM of DA, the concept of ROA is introduced. The advantages of ROA are that it can solve the complicated tasks, and it is less expensive. Moreover, it has the ability to obtain the global optimal solutions. Hence, the hybridisation of DA and ROA for DR detection is developed here, which is termed as TB – DA. In the past researches, more optimisation techniques were combined for introducing a new hybrid optimisation algorithm. These hybrid optimisation models have been produced promising results for specific search difficulties. This model makes use of the advantages of various

Figure 3. Solution encoding for optimal classification.

optimisation techniques in order to provide fast convergence. The convergence behaviour has been produced to be better than the traditional models [37]. The proposed TB – DA works on the basis of trail, which is counted when there is no improvement in the solution. The normal procedure of DA happens, if the trial is less than or equal to 5, and the solution is updated by the bypass rider based on Equation (35) if trial is greater than 5. The pseudo code of the proposed TB – DA is given in Algorithm 1.

5.3. Hybrid classifier

The hybridisation of DBN and NN is used to perform the detection of DR, in which the training algorithm is improved by the proposed TB – DA. This algorithm helps to update the weight of DBN and NN based on Figure 3, in which W_n^{NN} refers to the weight function of NN and W_n^{DBN} refers to the weight function of DBN.

5.3.1. DBN

It [38] consists of several layers similar to NN. The visible neurons are present in input layer and the hidden neurons are present in output layer. DBN employs Boltzmann network for obtaining the results effectively. The final outcome is denoted as opt and it captures binary format. The result consists of the probability of sinusoidal function $(BZ_{prb}(\lambda))$, and the corresponding equation is denoted in Equations (36) and (31). Here, the pseudo temperature parameter is denoted as pst that holds the noise level probability. The stochastic model is represented in Equation (38).

$$\mathrm{opt} = \begin{cases} 1 & \text{with } 1-BZ_{prb}(\lambda) \\ 0 & \text{with } BZ_{prb}(\lambda) \end{cases} \tag{36}$$

$$BZ_{prb}(\lambda) = \frac{1}{1+e^{\frac{-\lambda}{pst}}} \tag{37}$$

$$\lim_{pst\to 0^+} BZ_{prb}(\lambda) = \lim_{pst\to 0^+} \frac{1}{1+e^{\frac{-\lambda}{pst}}} = \begin{cases} 0 & \text{for } \lambda<0 \\ \frac{1}{2} & \text{for } \lambda=0 \\ 1 & \text{for } \lambda>0 \end{cases} \tag{38}$$

Boltzmann model is presented on the basis of Boltzmann distribution by the aim of accurate designing of input patterns. The energy of the Boltzmann system is used for configuring the neuron states and the corresponding equation is denoted in Equation (39).

$$\mathrm{BD}(\mathrm{nes}_1) = \sum_{p<q} \dot{M}_{p,q}\mathrm{nes}_p\mathrm{nes}_q - \beta_p\mathrm{nes}_q \tag{39}$$

In Equation (39), the neuron state is indicated by nes, the weight among the neurons is denoted as $\dot{M}_{p,q}$, and the biases of neurons are denoted as β. The Boltzmann system existing in DBN encircles the neurons by Equation (40).

$$\Delta\mathrm{BD}(c_p) = \sum_q \mathrm{nes}_p\dot{M}_{p,q} + \beta_p \tag{40}$$

Moreover, the configuration among the visible and the hidden neurons with respect to energy is denoted in Equations (41)–(43). In this, the binary state of visible and hidden neurons is denoted as vs_p and hd_q, the terms vw_p and hw_q are the bias weights of visible and hidden neurons, respectively. The assumed biases are denoted as Bi_p^* and Bi_q^*. Moreover, the training of restricted Boltzmann machine (RBM) reduces the taken probabilities in RBM learning as the parameter related to weight function restricts the probability distribution of the input data.

$$\mathrm{BD}(vs', hd) = -\sum_{(p,q)} \dot{M}_{p,q}vs_phd_q - \sum_p vs_pBi_p^* - \sum_q hd_qhw_q \tag{41}$$

$$\Delta\mathrm{BD}\left(vs_p, \vec{hd}\right) = \sum_q \dot{M}_{p,q}hd_q + Bi_p^* \tag{42}$$

$$\Delta\mathrm{BD}\left(\vec{vs}, hd_q\right) = \sum_q \dot{M}_{p,q}vs_p + Bi_p^* \tag{43}$$

Algorithm 1 . Pseudo code of proposed TB – DA

```
The entire solutions of dragonflies Y is initialised
The step vectors ΔY are initialised
while the final condition is not satisfied
if(trial ≤ 5)
  Update source of food & enemy
    update δ, sp, ag, ch, at and ds
  Compute Sp, Ag, Ch, At and Ds
  Update the radius of neighbours
  If a dragonfly has atleast one neighbouring dragonfly
    Equation (30) is used to update velocity vector
    Equation (31) is used to update position vector
  Else
    Equation (32) is used to update position vector
  end if
End if
Else
if(trial > 5)
  Update the solution by bypass rider using Equation (35)
End if
  Validate the updated solution by fitness evaluation
end while
```

In addition, RBM has the ability to allot the probability to each visible and hidden neuron with the help of obtained energy function shown in Equation (44). In this, the partition function is represented in Equation (45).

$$\mathrm{RB}'(vs', hd) = \frac{1}{\mathrm{PD}} e^{-F(vs', hd)} \tag{44}$$

$$\mathrm{PD} = \sum_{\vec{vs}, \vec{hd}} e^{-F'(vs', hd)} \tag{45}$$

The benchmark Boltzmann machine is defining the visible and hidden neurons automatically by measuring the difference of energy between the visible and hidden neurons is not equivalent to RBM.

NN: In multiple applications, NN [39,40] is very populous model for classification as it is flexible. The outcome of the hidden layer is calculated on the basis of Equation (46), in which the number of input neurons is denoted as $\mathrm{inp(co)}$. The overall output of the network is denoted in Equation (47), and the number of hidden neurons is represented as $\mathrm{hin(co)}$.

$$\bar{A}^{(A)} = \mathrm{ACF}\left(\tilde{W}^{(A)}_{(\hat{H}l)} + \sum_{k=1}^{\mathrm{inp(co)}} \tilde{W}^{(A)}_{(kl)} ZFit_{le*}\right) \tag{46}$$

$$\hat{B}_m = \mathrm{ACF}\left(\tilde{W}^{(B)}_{(\hat{H}m)} + \sum_{l=1}^{\mathrm{hin(co)}} \tilde{W}^{(B)}_{(lm)} \bar{A}^{(A)}\right) \tag{47}$$

In the above equations, the bias weight to the hidden neuron and the output neuron is denoted as $\tilde{W}^{(A)}_{(\hat{H}l)}$ and $\tilde{W}^{(B)}_{(\hat{H}m)}$, respectively. The weight from input neuron to hidden neuron and the weight from hidden neuron to output neuron is denoted as $\tilde{W}^{(A)}_{(kl)}$ and $\tilde{W}^{(B)}_{(lm)}$, respectively. The activation function is denoted as *ACF*. Moreover, for offering better training to NN, the weight $W^{NN}_n = \left\{\tilde{W}^{(A)}_{(\hat{H}l)}, \tilde{W}^{(B)}_{(\hat{H}m)}, \tilde{W}^{(A)}_{(kl)}, \tilde{W}^{(B)}_{(lm)}\right\}$ is chosen optimally by proposed TB – DA to minimise the error measure.

6. Results and discussions

6.1. Experimental procedure

The developed DR detection model was implemented by MATLAB 2018a, and the performance analysis was done. The dataset used for analysing the proposed model was DIARETDB1. Here, the population size was considered as 10 and the total number of iterations is 100. The performance of the proposed TB – DA-based DBN + NN was compared over Whale Optimisation Algorithm (WOA) [41], ROA [36], Modified Gear and Steering-based Rider Optimisation Algorithm (MGS – ROA) [42], DA [34] and Modified Levy Updated – Dragonfly Algorithm (MLU – DA)-[43] based DBN + NN for the measures 'accuracy, sensitivity, specificity, precision, false positive rate (FPR), false negative rate (FNR), NPV, false discover rate (FDR), F1 score and MCC'.

6.2. Performance metrics

The performance measures considered for experiment are given below. Here, the true positives and true negatives are denoted as tr^P and tr^N, respectively whereas the false positives and false negatives are indicated by fa^P and fa^N, respectively.

$$\mathrm{Accuracy} = \frac{tr^P + tr^N}{tr^P + tr^N + fa^P + fa^N} \tag{48}$$

$$\mathrm{Sensitivity} = \frac{tr^P}{tr^P + fa^N} \tag{49}$$

$$\mathrm{Specificity} = \frac{tr^N}{fa^P} \tag{50}$$

$$\mathrm{Precision} = \frac{tr^P}{tr^P + fa^P} \tag{51}$$

$$\mathrm{FPR} = \frac{fa^P}{fa^P + tr^N} \tag{52}$$

$$\mathrm{FNR} = \frac{fa^N}{tr^N + tr^P} \tag{53}$$

$$\mathrm{NPV} = \frac{fa^N}{fa^N + tr^N} \tag{54}$$

$$\mathrm{FDR} = \frac{fa^P}{fa^P + tr^P} \tag{55}$$

$$\mathrm{F1score} = \frac{\mathrm{Sensitivity} \bullet \mathrm{Precision}}{\mathrm{Precision} + \mathrm{Sensitivity}} \tag{56}$$

$$\mathrm{MCC} = \frac{tr^P \times tr^N - fa^P \times fa^N}{\sqrt{(tr^P + fa^P)(tr^P + fa^N)(tr^N + fa^P)(tr^N + fa^N)}} \tag{57}$$

6.3. Segmentation results

The experimental results of the 'optic disc segmentation, blood vessel segmentation and the abnormality segmentation' are given in Figure 4.

6.4. Performance analysis of optic disc

The performance analysis of optic disc by the proposed and the conventional heuristic-based DBN + NN is shown in Figure 5. From Figure 5(a), the accuracy of the improved TB – DA is determined exactly for all the learning percentages. At learning percentage 85, the accuracy of the implemented TB – DA is 12.5% better than MLU – DA, 16.1% better than WOA and 20% better than MGS – ROA-based DBN + NN. Moreover, the

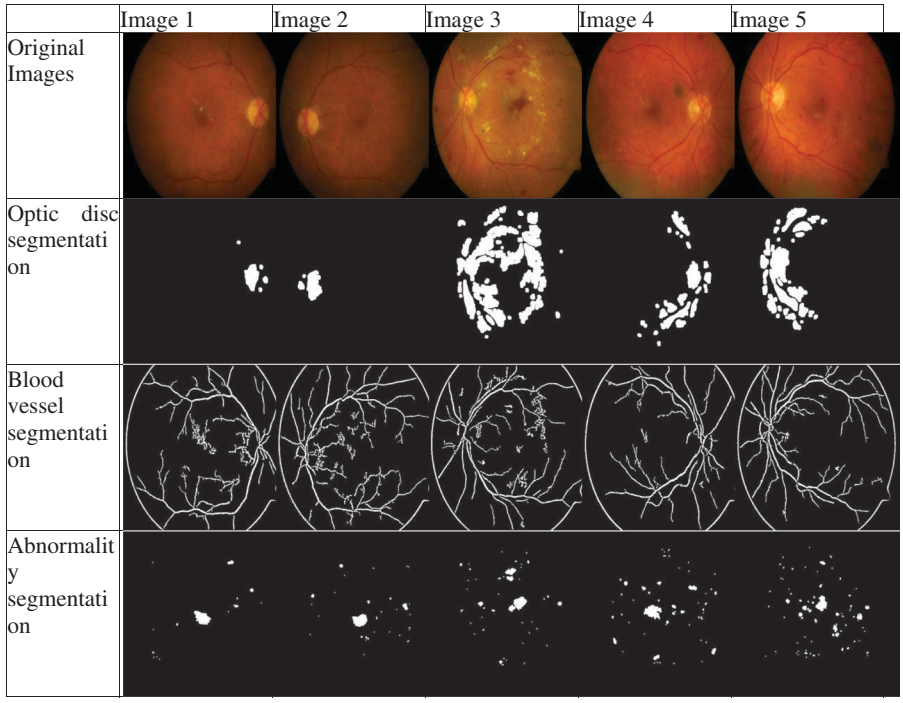

Figure 4. Segmentation results of optic disc, blood vessels and retinal abnormalities for five images.

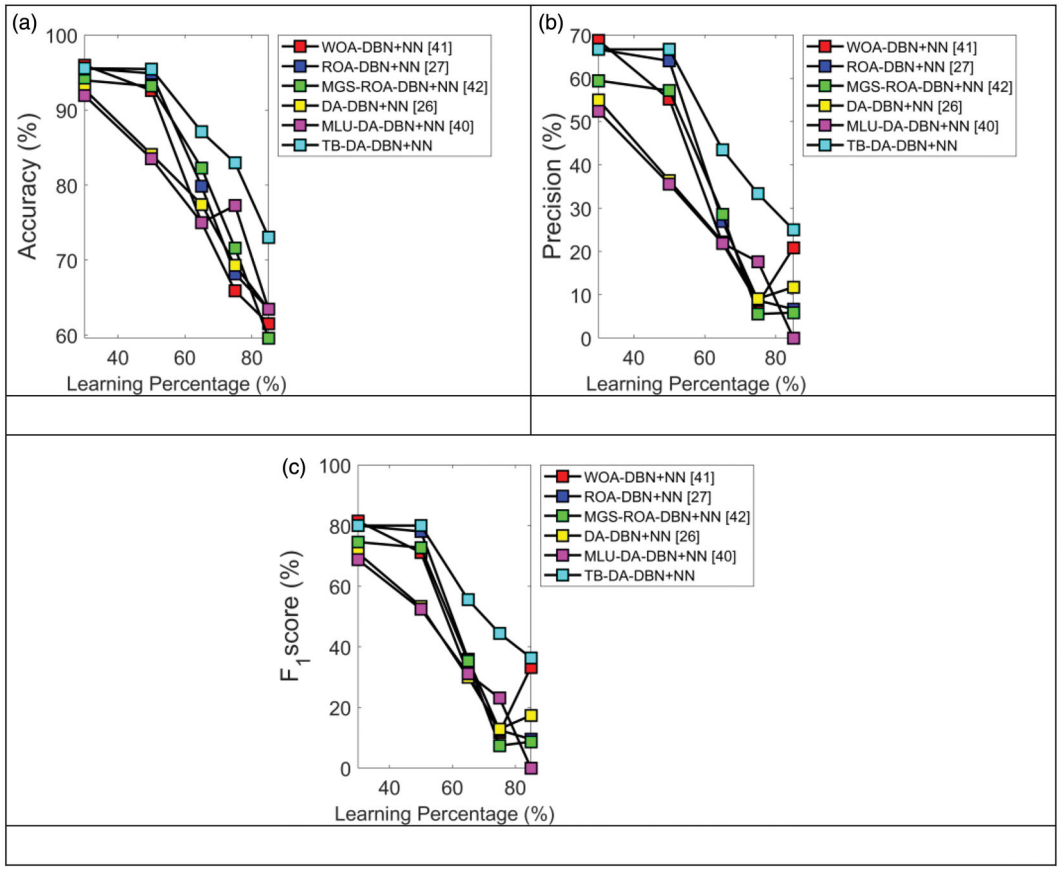

Figure 5. Performance analysis of diagnosing diabetic retinopathy by evaluating optic disc using three performance measures like (a) accuracy, (b) precision and (c) F1-score.

Table 2. Analysis on performance metrics for detecting diabetic retinopathy from optic disc using different heuristic-based hybrid classifier.

Performance measures	WOA – DBN + NN [35]	ROA – DBN + NN [38]	MGA – ROA – DBN + NN [39]	DA – DBN + NN [34]	MLU – DA – DBN + NN	TB – DA – DBN + NN
Accuracy	0.65909	0.68182	0.71591	0.69318	0.77273	0.82955
Sensitivity	0.22222	0.22222	0.11111	0.22222	0.33333	0.66667
Specificity	0.70886	0.73418	0.78481	0.74684	0.82278	0.8481
Precision	0.08	0.086957	0.055556	0.090909	0.17647	0.33333
FPR	0.29114	0.26582	0.21519	0.25316	0.17722	0.1519
FNR	0.77778	0.77778	0.88889	0.77778	0.66667	0.33333
NPV	0.70886	0.73418	0.78481	0.74684	0.82278	0.8481
FDR	0.92	0.91304	0.94444	0.90909	0.82353	0.66667
F1-score	0.11765	0.125	0.074074	0.12903	0.23077	0.44444
MCC	−0.0463	−0.03007	−0.07818	−0.02165	0.11982	0.38669

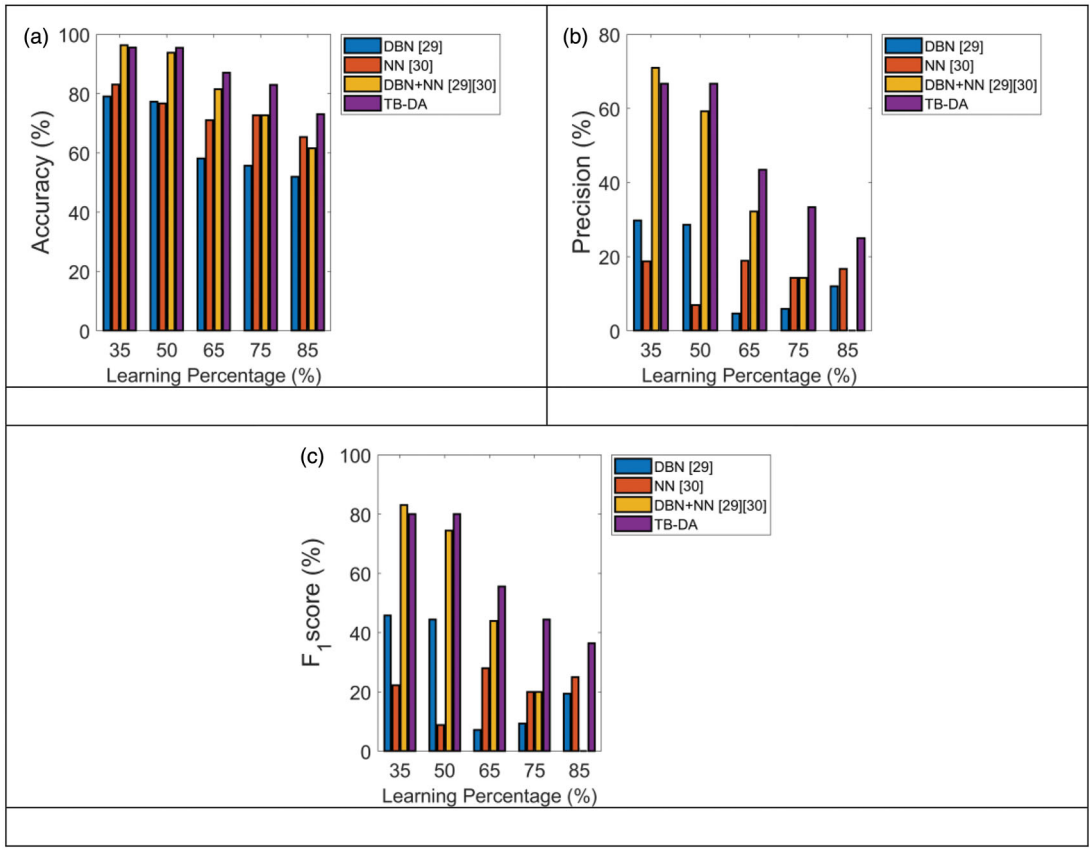

Figure 6. Performance analysis of diagnosing diabetic retinopathy by evaluating optic disc using different existing classifiers for performance measures like (a) accuracy, (b) precision and (c) F1-score.

precision of the improved TB – DA is 25% superior to WOA, 56% superior to DA, 72% superior to ROA, 76% superior to MGS – ROA and 100% superior to MLU – DA-based DBN + NN at learning percentage 85 and it is given in Figure 5(b). In addition, the other performance measures are also providing the best results for all the learning percentages. The overall performance analysis of the developed TB – DA is shown in Table 2. Here, the accuracy of the suggested TB – DA is 25.8% upgraded than WOA, 21.6% upgraded than ROA, 15.8% upgraded than MGS – ROA, 19.6% upgraded than DA and 7.3% upgraded than MLU – DA – DBN + NN. Finally, it is concluded that the performance of the improved TB – DA is superior to other heuristic algorithms. The classification performance of the developed TB – DA – DBN + NN is compared over the conventional machine learning algorithms with respect to learning percentage is given in Figure 6. From Figure 6(a), the accuracy of the TB – DA – DBN + NN is 25% improved than DBN + NN, 15.3% improved than NN and 50% improved than DBN at learning percentage 85. Similarly, in Figure 6(b), the precision of the recommended TB – DA – DBN + NN is 94.4% enhanced than DBN + NN and NN, and 77.1%

Table 3. Analysis on performance metrics for detecting diabetic retinopathy from optic disc using different existing classifiers.

Performance measures	DBN	NN	DBN + NN	TB – DA – DBN + NN
Accuracy	0.55682	0.72727	0.72727	0.82955
Sensitivity	0.22222	0.33333	0.33333	0.66667
Specificity	0.59494	0.77215	0.77215	0.8481
Precision	0.058824	0.14286	0.14286	0.33333
FPR	0.40506	0.22785	0.22785	0.1519
FNR	0.77778	0.66667	0.66667	0.33333
NPV	0.59494	0.77215	0.77215	0.8481
FDR	0.94118	0.85714	0.85714	0.66667
F1-score	0.093023	0.2	0.2	0.44444
MCC	–0.11378	0.074986	0.074986	0.38669

enhanced than DBN at learning percentage 75. Table 3 describes the overall performance of the improved TB – DA – DBN + NN over other machine learning algorithms. Here, the accuracy of the presented TB – DA – DBN + NN is 49% advanced than DBN, and 14.1% advanced than NN and DBN + NN. Hence, the best performance for the proposed TB – DA – DBN + NN has achieved for diagnosing DR.

6.5. Performance analysis of blood vessels

The performance evaluation of the proposed and the heuristic algorithms for all the learning percentages

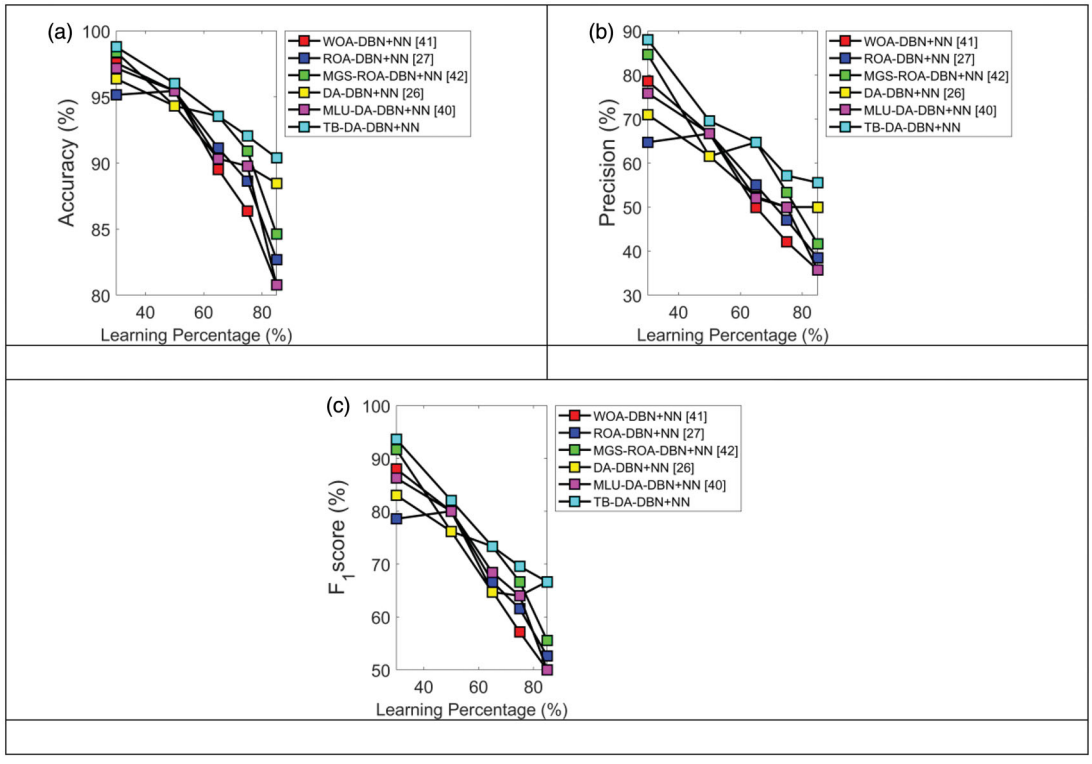

Figure 7. Performance analysis of diagnosing diabetic retinopathy by evaluating blood vessels using three performance measures like (a) accuracy, (b) precision and (c) F1-score.

Table 4. Analysis on performance metrics for detecting diabetic retinopathy from blood vessels using different heuristic-based hybrid classifier.

Performance measures	WOA – DBN + NN [35]	ROA – DBN + NN [38]	MGA – ROA – DBN + NN [39]	DA – DBN + NN [34]	MLU – DA – DBN + NN	TB – DA – DBN + NN
Accuracy	0.86364	0.88636	0.90909	0.89773	0.89773	0.92045
Sensitivity	0.88889	0.88889	0.88889	0.88889	0.88889	0.88889
Specificity	0.86076	0.88608	0.91139	0.89873	0.89873	0.92405
Precision	0.42105	0.47059	0.53333	0.5	0.5	0.57143
FPR	0.13924	0.11392	0.088608	0.10127	0.10127	0.075949
FNR	0.11111	0.11111	0.11111	0.11111	0.11111	0.11111
NPV	0.86076	0.88608	0.91139	0.89873	0.89873	0.92405
FDR	0.57895	0.52941	0.46667	0.5	0.5	0.42857
F1-score	0.57143	0.61538	0.66667	0.64	0.64	0.69565
MCC	0.55207	0.59479	0.64487	0.61877	0.61877	0.67346

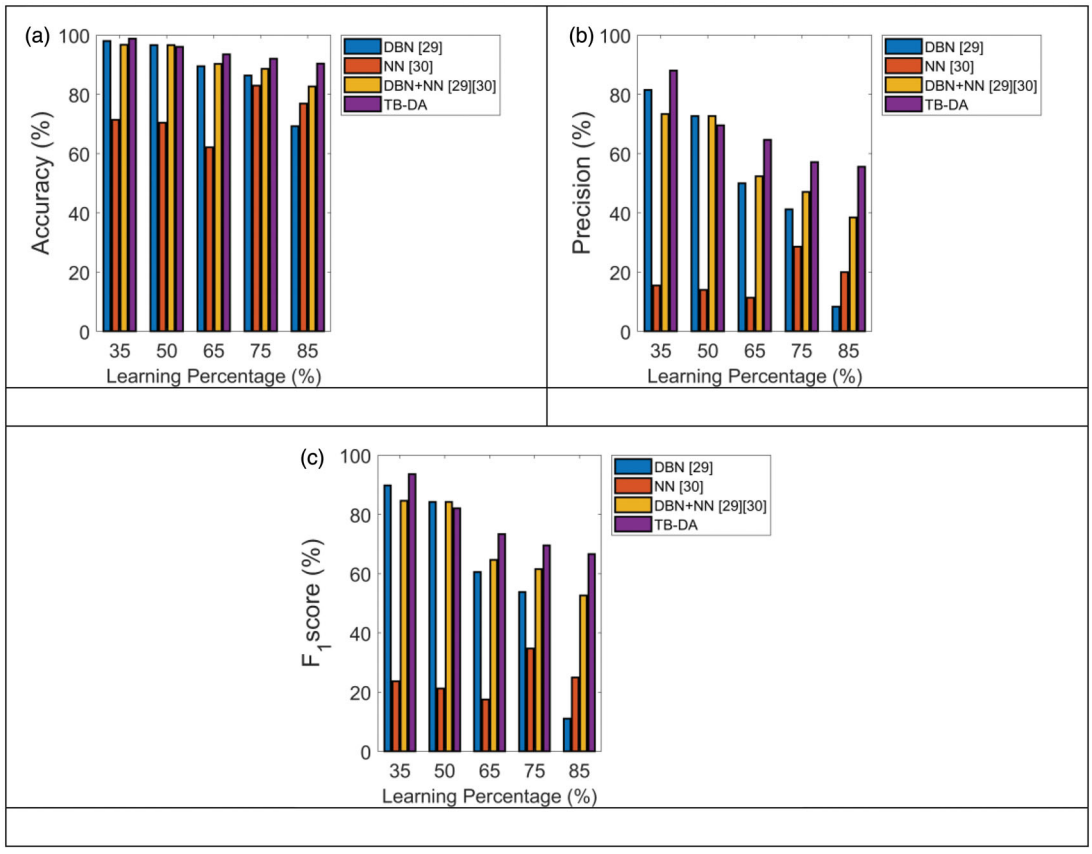

Figure 8. Performance analysis of diagnosing diabetic retinopathy by evaluating blood vessels using different existing classifiers for performance measures like (a) accuracy, (b) precision and (c) F1-score.

Table 5. Analysis on performance metrics for detecting diabetic retinopathy from blood vessels using different existing classifiers.

Performance measures	DBN	NN	DBN + NN	TB – DA – DBN + NN
Accuracy	0.86364	0.82955	0.88636	0.92045
Sensitivity	0.77778	0.44444	0.88889	0.88889
Specificity	0.87342	0.87342	0.88608	0.92405
Precision	0.41176	0.28571	0.47059	0.57143
FPR	0.12658	0.12658	0.11392	0.075949
FNR	0.22222	0.55556	0.11111	0.11111
NPV	0.87342	0.87342	0.88608	0.92405
FDR	0.58824	0.71429	0.52941	0.42857
F1-score	0.53846	0.34783	0.61538	0.69565
MCC	0.4998	0.26333	0.59479	0.67346

for segmenting blood vessels is shown in Figure 7. In Figure 7(a), the accuracy of the suggested TB – DA – DBN + NN is 1.1% exceeded than DA, 5.8% exceeded than MGS – ROA, 8.4% exceed than ROA and 11.1% exceeded than MLU – DA-based DBN + NN at learning percentage 85. On considering the learning percentage as 50 from Figure 7(b), the precision of the improved TB – DA – DBN + NN is 1.4% surpassed than MLU – DA, and 16.6% surpassed than DA – DBN + NN. The overall performance of the proposed TB – DA – DBN + NN and the existing algorithms is shown in Table 4. The accuracy of the suggested TB – DA – DBN + NN is 6.5% better than WOA, 3.8% better than ROA, 1.2% better than MGS – ROA, and 2.5% better than DA and MLU – DA. The classification performance of the modified TB – DA – DBN + NN compared over conventional classifiers is shown in Figure 8. Here, the accuracy of the improved TB – DA – DBN + NN is 2% better than DBN + NN, 41.4% better than NN and 1% better than DBN at learning percentage 35, which is shown in Figure 8(a). Moreover, the precision of the improved TB – DA – DBN + NN is shown in Figure 8(b), which is 45% superior to DBN + NN, 65.5% superior to NN and 82.7% superior to DBN at learning percentage 85. The overall classification analysis of the presented and the existing classifiers is shown in Table 5. The accuracy of the suggested TB – DA is 6.5% improved than DBN and DBN + NN, and 10.9% improved than NN. Hence, it is confirmed that the proposed TB – DA – DBN + NN is well suitable for detecting DR from blood vessels effectively.

6.6. Performance analysis of retinal abnormalities

The performance of the improved TB – DA – DBN + NN and the traditional algorithms concerning learning

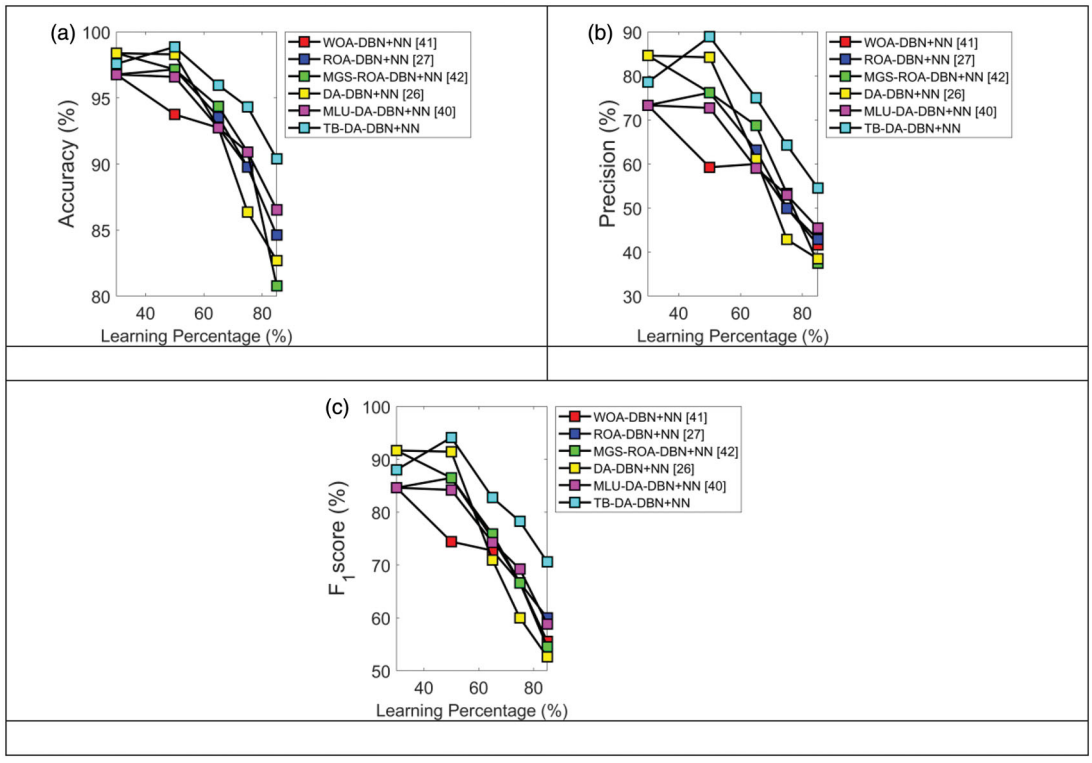

Figure 9. Performance analysis of diagnosing diabetic retinopathy by evaluating retinal abnormalities using three performance measures like (a) accuracy, (b) precision and (c) F1-score.

Table 6. Analysis on performance metrics for detecting diabetic retinopathy from retinal abnormalities using different heuristic-based hybrid classifier.

Performance measures	WOA – DBN + NN [35]	ROA – DBN + NN [38]	MGA – ROA – DBN + NN [39]	DA – DBN + NN [34]	MLU – DA – DBN + NN	TB – DA – DBN + NN
Accuracy	0.89773	0.89773	0.86364	0.90909	0.90909	0.94318
Sensitivity	1	1	1	0.88889	1	1
Specificity	0.88608	0.88608	0.8481	0.91139	0.89873	0.93671
Precision	0.5	0.5	0.42857	0.53333	0.52941	0.64286
FPR	0.11392	0.11392	0.1519	0.088608	0.10127	0.063291
FNR	0	0	0	0.11111	0	0
NPV	0.88608	0.88608	0.8481	0.91139	0.89873	0.93671
FDR	0.5	0.5	0.57143	0.46667	0.47059	0.35714
F1-score	0.66667	0.66667	0.6	0.66667	0.69231	0.78261
MCC	0.66561	0.66561	0.60289	0.64487	0.68978	0.776

percentages is shown in Figure 9. In Figure 9(a), the accuracy of the implemented TB – DA – DBN + NN is 3.4% enhanced than MLU – DA, 5.8% enhanced than ROA, 8.4% enhanced than DA and 11.1% enhanced than MGS – ROA – DBN + NN at learning percentage 85. When considering the learning percentage as 50, the precision of the improved TB – DA – DBN + NN is 5.8% superior to DA, 20% superior to MGS – ROA, 25% superior to MLU – DA and 50% superior to WOA. The overall performance of the implemented TB – DA – DBN + NN and the classical algorithms is shown in Table 6. The accuracy of the modified TB – DA – DBN + NN is 5% improved than WOA and ROA, 9.2% improved than MGS – ROA, 3.7% improved than DA and MLU – DA, which is given in Figure 9(b). The analysis of proposed and conventional machine learning algorithms is shown in Figure 10. In Figure 10(a), the accuracy of the implemented TB – DA – DBN + NN is 13.9% better than DBN + NN, 11.1% better than NN and 5.8% better than DBN at learning percentage 85. Moreover, from Figure 10(b), the precision of the implemented TB – DA – DBN + NN is 56.7% enhanced than DBN + NN, 48.7% enhanced than NN and 16% enhanced than DBN at learning percentage 85. The overall classification performance of the suggested TB – DA – DBN + NN and the conventional classifiers is shown in Table 7. In Table 7, the accuracy of the improved TB – DA is 2.4% better than DBN, 3.7% better than NN and 9.2% better than

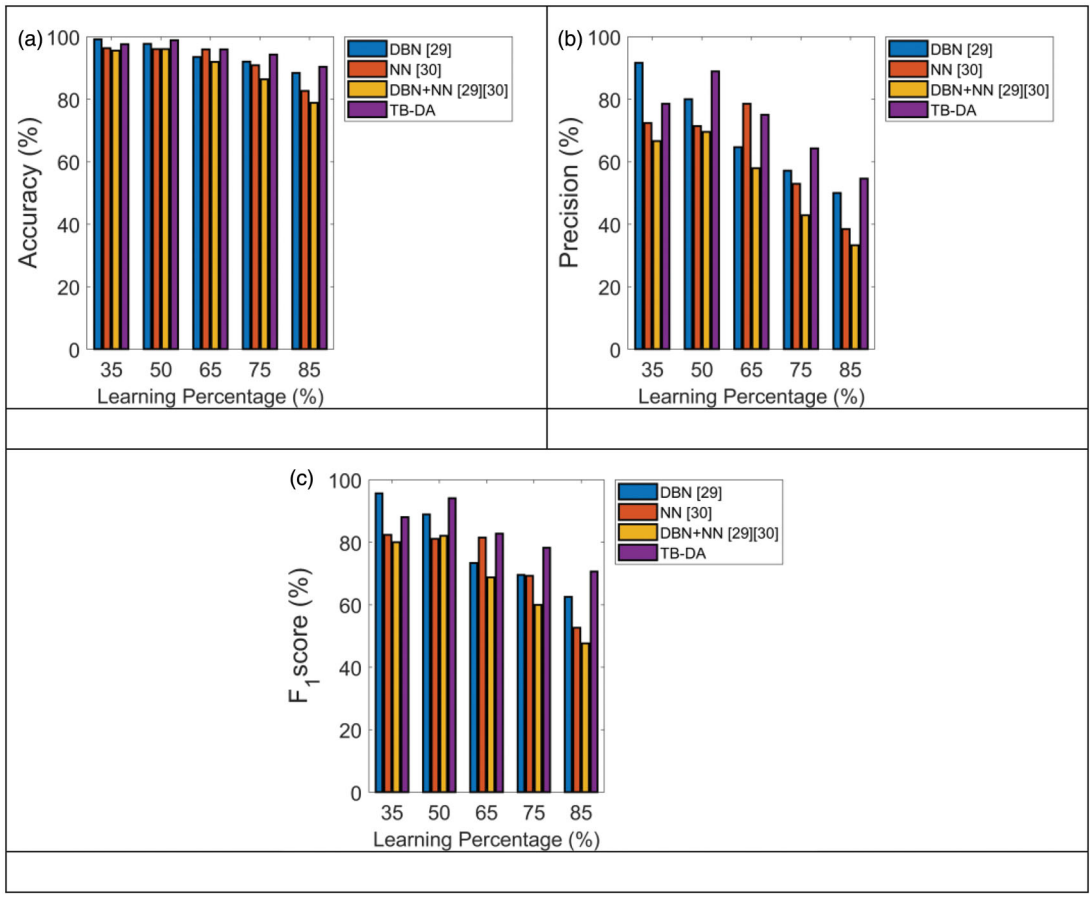

Figure 10. Performance analysis of diagnosing diabetic retinopathy by evaluating retinal abnormalities using different existing classifiers for performance measures like (a) accuracy, (b) precision and (c) F1-score.

Table 7. Analysis on performance metrics for detecting diabetic retinopathy from retinal abnormalities using different existing classifiers.

Performance measures	DBN	NN	DBN + NN	TB – DA – DBN + NN
Accuracy	0.92045	0.90909	0.86364	0.94318
Sensitivity	0.88889	1	1	1
Specificity	0.92405	0.89873	0.8481	0.93671
Precision	0.57143	0.52941	0.42857	0.64286
FPR	0.075949	0.10127	0.1519	0.063291
FNR	0.11111	0	0	0
NPV	0.92405	0.89873	0.8481	0.93671
FDR	0.42857	0.47059	0.57143	0.35714
F1-score	0.69565	0.69231	0.6	0.78261
MCC	0.67346	0.68978	0.60289	0.776

DBN + NN. Hence, it is verified that the proposed TB – DA – DBN + NN is performing well in diagnosing DR from retinal abnormailities.

7. Conclusion

The proposed DR detection model has consisted of three evaluations on the basis of optic disc, blood vessels and retinal abnormalities. At first, the image preprocessing was done by green channel conversion, and CLAHE. Later, the segmentation of optic disc was performed by open-close watershed transform, the blood vessel segmentation was done using grey level thresholding and abnormality segmentation was done by top hat transform and Gabor filtering techniques. From these segmented images, the features such as LBP, TEM, Shannon's and Kapur's entropy were extracted and this was given for optimal feature selection by the proposed TB – DA algorithm. The optimally selected features were subjected to a machine learning algorithm named DBN + NN with new TB – DA-based training. Finally, the analysis was performed based on optic disc, blood vessels and retinal abnormalities with the help of several performance metrics.

Disclosure statement

No potential conflict of interest was reported by the author(s).

References

[1] Singh N, Singh P. Stacking-based multi-objective evolutionary ensemble framework for prediction of diabetes mellitus. Biocybern Biomed Eng. 2020;40(1):1–22.

[2] Esteban S, Tablado M, Peper FE, et al. Development and validation of various phenotyping algorithms for Diabetes Mellitus using data from electronic health records. Comput Methods Programs Biomed. 2017; 152:53–70.
[3] Wu J, Diao YB, Li ML, et al. A semi-supervised learning based method: Laplacian support vector machine used in diabetes disease diagnosis. Interdiscip Sci. 2009;1(2):151–155.
[4] Solomon SD, Chew E, Duh EJ, et al. Diabetic retinopathy: a position statement by the American Diabetes Association. Diabetes Care. 2017;40(3):412–418.
[5] Yau JWY, Rogers SL, Kawasaki R, et al. Global prevalence and major risk factors of diabetic retinopathy. Diabetes Care. 2012;35(3):556–564.
[6] Murphree DH, Arabmakki E, Ngufor C, et al. Stacked classifiers for individualized prediction of glycemic control following initiation of metformin therapy in type 2 diabetes. Comput Biol Med. 2018;103:109–115.
[7] Zheng T, Xie W, Xu L, et al. A machine learning-based framework to identify type 2 diabetes through electronic health records. Int J Med Inform. 2017;97: 120–127.
[8] Aquino A, Gegundez-Arias ME, Marin D. Detecting the optic disc boundary in digital fundus images using morphological, edge detection, and feature extraction techniques. IEEE Trans Med Imaging. 2010;29(11): 1860–1869.
[9] Salazar-Gonzalez A, Kaba D, Li Y, et al. Segmentation of the blood vessels and optic disk in retinal images. IEEE J Biomed Health Inform. 2014;18(6):1874–1886.
[10] Cheung N, Mitchell P, Wong TY. Diabetic retinopathy. Lancet. 2010;376(9735):124–136.
[11] Goatman KA, Fleming AD, Philip S, et al. Detection of new vessels on the optic disc using retinal photographs. IEEE Trans Med Imaging. 2011;30(4):972–979.
[12] Zeng X, Chen H, Luo Y, et al. Automated diabetic retinopathy detection based on binocular siamese-like convolutional neural network. IEEE Access. 2019;7: 30744–30753.
[13] Ngo L, Han J. Multi-level deep neural network for efficient segmentation of blood vessels in fundus images. Electron Lett. 2017;53(16):1096–1098.
[14] Zhou L, Zhao Y, Yang J, et al. Deep multiple instance learning for automatic detection of diabetic retinopathy in retinal images. IET Image Process. 2018;12(4): 563–571.
[15] He K, Zhang X, Ren S, et al. Delving deep into rectifiers: surpassing human-level performance on ImageNet classification. Proceedings of the 2015 IEEE International Conference on Computer Vision (ICCV); 2015 Feb 6; Santiago. p. 1026–1034.
[16] Silver D, Huang A, Maddison CJ, et al. Mastering the game of Go with deep neural networks and tree search. Nature. 2016;529(7587):484–489.
[17] Sun Y, Liang D, Wang X, et al. DeepID3: face recognition with very deep neural networks. arXiv. 2015.
[18] Sun Y. The neural network of one-dimensional convolution-an example of the diagnosis of diabetic retinopathy. IEEE Access. 2019;7:69657–69666.
[19] Leeza M, Farooq H. Detection of severity level of diabetic retinopathy using Bag of features model. IET Comput Vis. 2019;13(5):523–530.
[20] Wan S, Liang Y, Zhang Y. Deep convolutional neural networks for diabetic retinopathy detection by image classification. Comput Electr Eng. 2018;72:274–282.
[21] Dashtbozorg B, Zhang J, Huang F, et al. Retinal microaneurysms detection using local convergence index features. IEEE Trans Image Process. 2018;27(7):3300–3315.
[22] Gao Z, Li J, Guo J, et al. Diagnosis of diabetic retinopathy using deep neural networks. IEEE Access. 2019;7: 3360–3370.
[23] Kumar D, Taylor GW, Wong A. Discovery radiomics With CLEAR-DR: interpretable computer aided diagnosis of diabetic retinopathy. IEEE Access. 2019;7: 25891–25896.
[24] Shaik F, Sharma AK, Ahmed SM. Hybrid model for analysis of abnormalities in diabetic cardiomyopathy and diabetic retinopathy related images. SpringerPlus. 2016;5(1):507.
[25] Costa P, Galdran A, Smailagic A, et al. A weakly-supervised framework for interpretable diabetic retinopathy detection on retinal images. IEEE Access. 2018;6: 18747–18758.
[26] Sonali S, KumarSingh A, Ghrera SP, et al. An approach for de-noising and contrast enhancement of retinal fundus image using CLAHE. Opt Laser Technol. 2019; 110:87–98.
[27] Madhumitha S, Manikandan M. Quantitative analysis of marker-based watershed image segmentation. Curr Sci. 2018;114(5):1007–1013.
[28] Dey S, Bhattacharyya S, Maulik U. Quantum inspired genetic algorithm and particle swarm optimization using chaotic map model based interference for gray level image thresholding. Swarm Evol Comput. 2014; 15:38–57.
[29] Abdullah Yahya A, Tan J, Hu M. A novel model of image segmentation based on watershed algorithm. Adv Multimed. 2013;2013:1–8.
[30] Khaleefah SH, Mostafa SA, Mustapha A, et al. The ideal effect of Gabor filters and Uniform Local Binary Pattern combinations on deformed scanned paper images. J King Saud Univ - Comput Inf Sci. 2019. DOI: 10.1016/j.jksuci.2019.07.012
[31] Liao S, Law MWK, Chung ACS. Dominant local binary patterns for texture classification. IEEE Trans Image Process. 2009;18(5):1107–1118.
[32] Gupta R, Undrill PE. The use of texture analysis to delineate suspicious masses in mammography. Phys Med Biol. 1995;40(5):835–855.
[33] Mookiah MRK, Acharya UR, Martis RJ, et al. Evolutionary algorithm based classifier parameter tuning for automatic diabetic retinopathy grading: a hybrid feature extraction approach. Knowl Based Sys. 2013;39:9–22.
[34] Jafari M, Bayati Chaleshtari MH. Using dragonfly algorithm for optimization of orthotropic infinite plates with a quasi-triangular cut-out. Eur J Mech A: Solids. 2017;66:1–14.
[35] Pedersen MEH, Chipperfield AJ. Simplifying particle swarm optimization. Appl Soft Comput. 2010;10(2): 618–628.

[36] Binu D, Kariyappa BS. RideNN: a new rider optimization algorithm-based neural network for fault diagnosis in analog circuits. IEEE Trans Instrum Meas. 2019; 68(1):2–26.

[37] Marsaline Beno M, Valarmathi IR, Swamy SM, et al. Threshold prediction for segmenting tumour from brain MRI scans. Int J Imaging Syst Technol. 2014; 24(2):129–137.

[38] Liu Y, Zhou H, Tsung F, et al. Real-time quality monitoring and diagnosis for manufacturing process profiles based on deep belief networks. Comput Ind Eng. 2019;136:494–503.

[39] Fernández-Navarro F, Carbonero-Ruz M, Becerra Alonso D, et al. Global sensitivity estimates for neural network classifiers. IEEE Trans Neural Netw Learn Syst. 2017;28(11):2592–2604.

[40] George A, Rajakumar BR. On hybridizing fuzzy min max neural network and firefly algorithm for automated heart disease diagnosis. Proceedings of the Fourth International Conference on Computing, Communications and Networking Technologies; July 2013, Tiruchengode, India.

[41] Mirjalili S, Lewis A. The whale optimization algorithm. Adv Eng Softw. 2016;95:51–67.

[42] Jadhav AS, Patil PB. Optimal feature selection-based diabetic retinopathy detection using improved rider optimization algorithm enabled with deep learning. Evol Intel. 2020. DOI:10.1007/s12065-020-00400-0

[43] Jadhav AS, Patil PB. Computer aided diabetic retinopathy diagnostic model using optimal thresholding merged with neural network. International Journal of Intelligent Computing and Cybernetics. 2020. DOI:10.1108/IJICC-11-2019-0119